Author for correspondence:
Giuseppe Tronci
e-mail: g.tronci@leeds.ac.uk

THE ROYAL SOCIETY
PUBLISHING

Multi-scale mechanical characterization of highly swollen photo-activated collagen hydrogels

Giuseppe Tronci[1,3], Colin A. Grant[5], Neil H. Thomson[2,4], Stephen J. Russell[1] and David J. Wood[3]

[1]Nonwovens Research Group, School of Design, and [2]Molecular and Nanoscale Physics, School of Physics and Astronomy, University of Leeds, Leeds LS2 9JT, UK
[3]Biomaterials and Tissue Engineering Research Group, School of Dentistry, and [4]Biomineralisation Research Group, School of Dentistry, University of Leeds, Leeds LS2 9LU, UK
[5]Advanced Materials Engineering RKT Centre, School of Engineering, University of Bradford, Bradford BD7 1DP, UK

Biological hydrogels have been increasingly sought after as wound dressings or scaffolds for regenerative medicine, owing to their inherent biofunctionality in biological environments. Especially in moist wound healing, the ideal material should absorb large amounts of wound exudate while remaining mechanically competent *in situ*. Despite their large hydration, however, current biological hydrogels still leave much to be desired in terms of mechanical properties in physiological conditions. To address this challenge, a multi-scale approach is presented for the synthetic design of cyto-compatible collagen hydrogels with tunable mechanical properties (from the nano- up to the macro-scale), uniquely high swelling ratios and retained (more than 70%) triple helical features. Type I collagen was covalently functionalized with three different monomers, i.e. 4-vinylbenzyl chloride, glycidyl methacrylate and methacrylic anhydride, respectively. Backbone rigidity, hydrogen-bonding capability and degree of functionalization (F: 16 ± 12–91 ± 7 mol%) of introduced moieties governed the structure–property relationships in resulting collagen networks, so that the swelling ratio (SR: 707 ± 51–1996 ± 182 wt%), bulk compressive modulus (E_c: 30 ± 7–168 ± 40 kPa) and atomic force microscopy elastic modulus (E_{AFM}: 16 ± 2–387 ± 66 kPa) were readily adjusted. Because of their remarkably high swelling *and* mechanical properties, these tunable collagen hydrogels may be further exploited for the design of advanced dressings for chronic wound care.

1. Introduction

Hydrogels are three-dimensional networks based on hydrophilic homo-polymers, co-polymers or macromers, which are cross-linked to form insoluble polymer matrices [1,2]. Following the large amount of water absorbed by the dry polymer network in physiological aqueous conditions, the resulting gels are typically soft and compliant. This behaviour results from the thermodynamic compatibility of the dry polymer with water, the presence of junction knots, as well as the low glass transition temperature (T_g) of the polymer network in hydrated conditions. In view of these features, the potential application of hydrogels in healthcare was first realized in the early 1960s, with the development of poly(2-hydroxyethyl methacrylate) gels as a contact lens material [3]. Subsequently, hydrogels have been designed based on other synthetic polymers, such as poly(ethylene glycol) [4] and poly (vinyl alcohol) [5], for various biomedical applications, including controlled drug delivery [6], wound care [7] and diabetes treatments [8]. Most recently, the design of multi-functional hydrogels based on naturally occurring biomacromolecules has received a great deal of

attention due to the fact that these systems can mimic the extracellular matrix (ECM) of biological tissues [9,10], thereby enabling selective drug sequestration [11] and extended engraftment of transplanted cells [12].

Collagen is the main protein of the human body, ruling structure, function and shape of biological tissues. Also in the light of their unique molecular organization, collagen hydrogels have been widely applied for the design of vascular grafts [13], biomimetic scaffolds for regenerative medicine [14] and non-woven architectures for wound healing [15]. Especially in moist wound healing [16,17], collagen hydrogels have been receiving a great deal of attention, since they can absorb large amounts of water following swelling, while being enzymatically degraded by matrix metalloproteinases (MMPs) present at the wound site. Both functionalities are key to the design of advanced wound dressings, aiming (i) to maintain defined wound temperature and metabolic rate [18] and (ii) to control MMP levels (probably responsible for delayed healing) at the wound site [19]. Following equilibration with medium, however, collagen hydrogels often exhibit limited mechanical properties and processability [20], potentially resulting in damage of the material upon handling. As a result, non-controllable macroscopic properties are observed, whereby a trade-off between the degree of swelling and mechanical properties critically impairs the successful translation of such materials into the clinic [21], especially in chronic wound care [22].

In its monomeric form, the collagen molecule is based on three left-handed polyproline chains, each one containing the repeating unit Gly-X-Y, where X and Y are predominantly proline (Pro) and hydroxyproline (Hyp), respectively [23]. The three chains are staggered to one another by one amino acid residue and are twisted together to form a right-handed triple helix (300 nm in length, 1.5 nm in diameter) [24]. *In vivo*, triple helices can aggregate in a periodic staggered array to form collagen fibrils, fibres and fascicles, which are stabilized via covalent cross-links. Despite the prevalence of such a hierarchical self-assembled structure *in vivo*, collagen extracted from biological tissues is mechanically unstable in aqueous environments, owing to the fact that its organization and chemical composition can only partially be reproduced *in vitro* [25]. Fibrillogenesis can be induced by exposing triple helical collagen to physiological conditions; however, native hydrogen and covalent bonds are partially broken following collagen isolation *ex-vivo*, so that collagen hierarchical organization and resulting mechanical properties are affected. Cross-linking methods based on either covalent [26–28] or physical [29–31] linkages, gelling strategies employing, for example, fibrillated protein backbones [32], as well as scaffold fabrication techniques [33] can be applied to collagen to enhance mechanical behaviour. Such methods offer elegant but still limited solutions to the stabilization of biomimetic collagen structures.

In order to address these challenges, rational approaches to hydrogel design should be developed, whereby systematic investigations of the hydrated mechanical properties should be carried out at all levels of hierarchical organization. Here, the interaction between building blocks, the effect of each building block and contributions of different phases (e.g. protein backbone, cross-linker, swelling medium) to the overall mechanical performance should be explored [34]. At the fibrillar level, however, nanoscale imaging [35] and micro-mechanical measurements on collagen materials have only recently become possible. Grant *et al.* [36] carried out atomic force microscopy (AFM) tapping mode and force volume measurements on reconstituted type I collagen fibrils. Resulting fibrils revealed the characteristic periodic banding (67 nm) pattern in either air or sodium phosphate buffer, while a three order magnitude decrease in elastic modulus (E_{AFM}: 1.85 ± 0.49 GPa → 1.18 ± 0.14 MPa) was observed in the hydrated sample as compared with the dry-state elastic modulus [37]. Obtained nanoindentation values were comparable to the tensile ones measured via a microelectromechanical system [38], while the remarkable decrease in hydrated micromechanical properties, probably ascribed to the formation of hydrogen bonds within collagen molecules, was macroscopically associated with a two-fold swelling of the collagen fibril. Aiming to develop novel architectures for tissue engineering scaffolds, Carlisle *et al.* [39] probed fibre micromechanical properties in electrospun type I collagen. The resulting elastic modulus proved to be in the same range as that of reconstituted collagen fibrils (E_{AFM}: 2.8 ± 0.4 GPa); however, measurements were only carried out in the dry state, so that the effects of electrospinning and electrospinning solvent on collagen conformation and wet-state stability were not addressed. In an effort to study the effect of intermolecular covalent cross-links, Svensson *et al.* [40] successfully measured significantly enhanced mechanical properties (E_{AFM}: 2.2 ± 0.9 GPa → 3.5 ± 0.4 GPa) in hydrated collagen fibrils with increased levels of tendon cross-link maturity, while no effect of environmental salts was detected [41]. Going towards higher levels of tissue hierarchy, the mechanical properties of collagen fibrils and tendons were also compared, whereby different values of elastic modulus (E_{fibril}: 2.0 ± 0.5 GPa; E_{tendon}: 2.8 ± 0.3 GPa) were observed [42]. Ultimately, AFM was applied on carbodiimide cross-linked type I collagen gels in order to probe the effect of cross-linking on fibrillar organization [43]. Here, tensile properties were significantly improved, although fibril formation proved to be suppressed when cross-linking was carried out simultaneously with collagen fibrillogenesis. From all the aforementioned examples, it appears rather clear that, while recent developments on AFM and mechanical testing enabled successful mechanical and structural characterization, collagen-based hydrogels with defined relationships between the molecular, microscopic and macroscopic scale are still only partially accomplished. This is, on the one hand, due to the technical limitations related to the resolution of highly swollen networks via AFM and, on the other hand, due to the fact that chemo-selective and tunable functionalization of collagen is still very challenging.

The aim of this work was to study the structure–property–function relationships in photo-activated collagen hydrogels to investigate their potential applicability in chronic wound care. By covalently functionalizing type I collagen with photo-active compounds of varied molecular weight, backbone rigidity and hydrophilicity [44], i.e. 4-vinylbenzyl chloride (4VBC), glycidyl methacrylate (GMA) and methacrylic anhydride (MA), hydrogels were successfully accomplished following collagen precursor photo-activation. By controlling the network molecular architecture, the swelling and mechanical properties from the nano- up to the macro-scale were expected to be adjusted. We selected photo-activated cross-linking for the design of collagen hydrogels since this strategy has been successfully applied to the formation of synthetic polymer systems whose biocompatibility, tunability and control of material properties have been widely reported [1–8,45]. Compared with other synthetic strategies, photo-activated cross-linking provides rapid reaction rates

with controlled temporal and spatial features, while also enabling the encapsulation of cells and drugs in the polymer system [46,47]. By applying the knowledge gained with synthetic and linear biomacromolecular networks, we investigated how photo-activated cross-linking could be applied to triple helical collagen, aiming to accomplish collagen-based hydrogels with programmed structure–property relationships.

2. Material and methods

2.1. Materials

GMA, 4VBC, MA and 2,4,6-trinitrobenzenesulfonic acid (TNBS) were purchased from Sigma-Aldrich. Rat tails were supplied by the School of Dentistry, University of Leeds (UK). All the other chemicals were purchased from Sigma-Aldrich. Type I collagen was isolated in-house via acidic treatment of rat tail tendons [44].

2.2. Functionalization of collagen

Type I collagen (0.25 wt%, 100 g solution) was stirred in 10 mM hydrochloric acid solution at room temperature until a clear solution was obtained. Solution pH was neutralized to pH 7.4 and either GMA, 4VBC or MA was added to the reaction mixture with a 10–50 molar excess with respect to collagen lysines (e.g. 50 mmol monomer per mmol of collagen lysine) depending on the specific sample formulation. An equimolar amount of triethylamine (with respect to the amount of monomer previously added) and 1 wt% of Tween-20 (with respect to the initial solution volume) were added. After 24 h reaction, the mixture was precipitated in 10–15 volume excess of pure ethanol and stirred for 2 days. Ethanol-precipitated functionalized collagen was recovered by centrifugation and air-dried.

2.3. Photo-activation and network formation

GMA- and MA-functionalized collagens (0.8 wt%) were stirred in 1 wt% I2959–phosphate-buffered saline (PBS) solution. The resulting solutions were poured onto Petri dishes and incubated in a vacuum desiccator to remove air bubbles; this was followed by UV irradiation (Spectroline, 346 nm, 9 mW cm^{-2}) for 30 min on each dish side. Networks based on 4VBC-functionalized collagen were prepared following the same protocol, except that the solution was prepared in 1 wt% I2959–10 mM hydrochloric acid. Formed hydrogels were washed in distilled water and dehydrated via ascending series of ethanol solutions.

2.4. Chemical and structural characterization

The degree of collagen functionalization (F) was determined by TNBS colorimetric assay [48], according to the following equations:

$$\frac{mol(Lys)}{g(collagen)} = \frac{2 \times Abs(346\,nm) \times 0.02}{1.46 \times 10^4 \times b \times x} \qquad (2.1)$$

and

$$F = 1 - \frac{mol(Lys)_{Funct.Collagen}}{mol(Lys)_{Collagen}}, \qquad (2.2)$$

where Abs(346 nm) is the absorbance value at 346 nm, 0.02 is the volume of sample solution (in litres), 1.46×10^4 is the molar absorption coefficient for 2,4,6-trinitrophenyl lysine (in $M^{-1} \cdot cm^{-1}$), b is the cell path length (1 cm) and x is the sample weight. Here mol(Lys)$_{Collagen}$ and mol(Lys)$_{Funct.Collagen}$ represent the total molar content of free amino groups in native and functionalized collagen, respectively. The nomenclature (Lys) is hereby used to recognize that lysines make the highest contribution to the molar content of collagen free amino groups, although contributions from hydroxylysines and amino termini are also taken into account.

Besides TNBS, collagen functionalization was also investigated by ^{1}H-NMR spectroscopy (Bruker Avance spectrophotometer, 500 MHz) by dissolving 5–10 mg of dry samples in 1 ml deuterium oxide. Attenuated total reflectance Fourier-transform infrared (ATR FT-IR) was carried out on dry samples using a Perkin-Elmer Spectrum BX spotlight spectrophotometer with diamond ATR attachment. Scans were conducted from 4000 to 600 cm^{-1} with 64 repetitions averaged for each spectrum.

Circular dichroism (CD) spectra of functionalized samples were acquired with a ChirascanCD spectrometer (Applied Photophysics Ltd) using 0.2 mg ml^{-1} solutions in 10 mM HCl. Sample solutions were collected in quartz cells of 1.0 mm path length, whereby CD spectra were obtained with 4.3 nm band width and 20 nm min^{-1} scanning speed. A spectrum of the 10 mM HCl control solution was subtracted from each sample spectrum.

Wide angle X-ray scattering (WAXS) measurements were carried out on dry samples with a Bruker D8 Discover (40 kV, 30 mA, X-ray wavelength: $\lambda = 0.154$ nm). The detector was set at a distance of 150 mm covering 2Θ from $5°$ to $40°$. The collimator was 2.0 mm and the exposure time was 10 s per frame. Collected curves were subtracted from the background (no sample loaded) curve and fitted with polynomial functions ($R^2 > 0.95$).

2.5. Scanning electron microscopy

Fully hydrated hydrogels were investigated via a cool stage SEM (JEOL SM-35) in order to explore the inner morphology of collagen hydrogels. Samples were mounted onto 10 mm stubs fitting a cool stage set at 10°C inside the specimen chamber of a Hitachi S-3400N VP-SEM. A drop of distilled water was placed around the sample, whereas the chamber pressure and stage temperature were correlatively decreased to 70 Pa and $-20°$C, respectively, enabling the use of water vapour as imaging gas. SEM images were captured via backscattered electron detection at 10 kV and 12–13 mm working distance.

2.6. Swelling tests

A total of 2–5 mg of dry sample was placed in 1 ml of either distilled water or PBS under mild shaking. Upon equilibrium with water, the SR was calculated according to the following equation:

$$SR(\%) = \frac{W_s - W_d}{W_d} \times 100, \qquad (2.3)$$

where W_s and W_d are the swollen and dry sample masses, respectively. Swollen samples were paper blotted prior to measurement of W_s.

2.7. Compression tests

Water-equilibrated hydrogel discs (Ø: 0.8 cm) were compressed at room temperature with a compression rate of 3 mm min^{-1} (Instron ElectroPuls E3000). A 250 N load cell was operated up to sample break. Four replicas were employed for each composition and the results expressed as the mean $\pm$ s.d.

2.8. Atomic force microscopy indentation and scanning

Gel samples were glued using a blue-light-activated adhesive to a standard microscope slide and placed on the sample stage of an MFP-3D AFM (Asylum Research, Santa Barbara, CA, USA) before placing approximately 100 µl of ultrapure water (18.4 MΩ·cm) on the gel surface. AFM imaging was carried out with either tapping or contact mode using a V-shaped silicon nitride cantilever (Hydra6V series; AppNano, Santa Clara, CA, USA) with a spring constant of approximately 0.3 N m^{-1} and a tip radius of 15 nm, which was independently confirmed

using a standard calibration grid. Following laser alignment, calibration of the detector sensitivity and the cantilever spring constant ($k \sim 0.32$ N m^{-1}) using the thermal method was made [49]. Roughness values (R_a, R_q) were computationally calculated using the MFP-3D software from Asylum. These involve the summation and average (R_a) and square root of height squared (R_q) for all height data above/below a statistically determined centre line.

Force volume measurements were made in organized arrays (50×50) of indentations at a piezo velocity of $2 \, \mu m \, s^{-1}$. The elastic modulus was estimated using a linear elastic Hertzian-based theory for a conical indenter

$$F = \frac{2}{\pi} \left(\frac{E}{1 - \nu^2} \right) \delta^2 \tan \alpha, \tag{2.4}$$

where ν is Poisson's ratio and is assigned a value of 0.5 (i.e. incompressible), δ is the indentation depth and α is the half cone angle of the probe ($36°$).

2.9. Cell viability

L929 cells were incubated in a 5-chloromethylfluorescein diacetate solution (CellTrackerGreen CMFDA, Invitrogen) for 45 min. The dye working solution was replaced with serum-free medium and cells incubated for 45 min intervals twice. Labelled cells were seeded onto ethanol-treated hydrogel discs (Ø: 8 mm; h: 3 mm; 10^4 cells sample^{-1}) for 48 h followed by optical observation via fluorescent miscroscopy. Other than that, an extract cytotoxicity assay was also conducted (EN DIN ISO standard 10993–5) in order to further investigate the material compatibility with L929 cells. A total of 0.1 mg of ethanol-treated hydrogel was incubated in 1 ml cell culture medium (Dulbecco's modified Eagle medium; DMEM) at $37°$C. After 72 h incubation, the sample extract was recovered and applied to 80% confluent L929 mouse fibroblasts cultured on a polystyrene 96-well plate. Dimethyl sulfoxide was used as the negative control, while DMEM was applied as the positive control. Cell morphology was investigated using a transmitted light microscope in phase contrast mode.

3. Results and discussion

Sample nomenclature is as follows: functionalized collagen precursors are identified as 'CRT-XXYY', where 'CRT' indicates type I collagen isolated in-house from rat tails; 'XX' identifies the monomer reacted with CRT (either 4VBC, GMA or MA); 'YY' describes the monomer/lysine molar ratio used in the functionalization reaction. Collagen hydrogels are identified as 'CRT-XXYY*', where 'CRT', 'XX' and 'YY' have the same meanings as previously mentioned, while '*' indicates that the sample results from the photo-activation of a collagen precursor.

3.1. Synthesis of functionalized collagen precursors and networks

In-house isolated type I collagen was functionalized with varied vinyl moieties in order to obtain covalent hydrogel networks following photo-activation of resulting precursors (figure 1a). Collagen functionalization can occur via nucleophilic reaction of free amino groups, e.g. the ones found in lysine (Lys), hydroxylysine and arginine as well as collagen amino termini. At the same time, arginine is unlikely to react in these conditions, owing to the high pK_a (approx. 12.5) and the resonance stabilization of the protonated guanidium group.

4VBC and GMA were selected as rigid, aromatic monomer and flexible, aliphatic monomer, respectively, while MA was chosen as short, methacrylic compound. ^{1}H-NMR (electronic supplementary material, figure S1) and TNBS colorimetric assay (figure 1d) confirmed the covalent functionalization in all three collagen products; the presence of the characteristic geminal proton peaks of MA (5.3 and 5.6 ppm) [50,51] were clearly identified in the ^{1}H-NMR spectrum of sample CRT-MA25, in line with spectral information obtained via ATR-FTIR (electronic supplementary material, figure S2). A tunable number of lysine amino groups was covalently functionalized, based on the monomer type and the molar excess of monomer with respect to the collagen lysine content (R, figure 1d) in the reacting mixture. These results probably reflect the different reactivity and solubility of selected monomers in water, so that the degree of collagen functionalization (F) was successfully adjusted in the range of 16 ± 12–91 ± 7 mol%.

Further to the chemical yield, the impact of functionalization on collagen triple helix organization was also addressed, since this is an important molecular feature influencing collagen stability, mechanical properties and biofunctionality [52–54]. Far-UV CD spectra of functionalized collagens displayed a positive peak at 221 nm, associated with collagen triple helices, and a negative peak at 198 nm, describing polyproline chains, as in the case of native collagen spectrum (figure 1b). Importantly, the magnitude ratios of the positive to negative peak (RPN) in functionalized collagen spectra (figure 1d) were found to be comparable (RPN: 0.092–0.127) to the value of native collagen (RPN: 0.117) [55,56], indicating that the triple helix architecture could be preserved in photo-active collagen products depending on the type and extent of collagen functionalization. Interestingly, sample CRT-4VBC25 revealed lower RPN and slightly higher F values than sample CRT-4VBC10 (figure 1d). Normalization of corresponding RPN values with respect to the RPN value of native collagen resulted in triple helix contents of 79% and 98% in samples CRT-4VBC25 and CRT-4VBC10, respectively. This observation may therefore suggest that the additional functionalization of collagen with bulky 4VBC aromatic moieties is likely to result in a detectable reduction of collagen triple helices, due to the inability of 4VBC moieties to mediate hydrogen bonds (as crucial bonds to triple helix stability) [57]. Other than CD, corresponding collagen networks were also analysed via WAXS in order to explore the organization of functionalized collagen in the cross-linked state. Obtained WAXS spectra displayed characteristic peaks related to the collagen intermolecular lateral packing ($d \sim 1.1$ nm, $2\Theta \sim 8°$), isotropic amorphous region ($d \sim 0.5$ nm, $2\Theta \sim 20°$) and axial polyproline periodicity ($d \sim 0.29$ nm, $2\Theta \sim 31°$), as observed in the spectrum of native collagen (figure 1c). The integration ratio between the peak related to collagen intermolecular lateral packing (describing the presence of collagen triple helices) and the overall WAXS spectrum was determined in order to quantify the triple helix content in functionalized collagen networks. Normalization of resulting integration ratios with respect to the integration ratio in native collagen indicated that at least 73% of native triple helix content was successfully preserved, confirming previous CD results. In contrast to that, a gelatin control was also analysed during the measurements, whereby only 2% of collagen-like triple helices was detected, in agreement
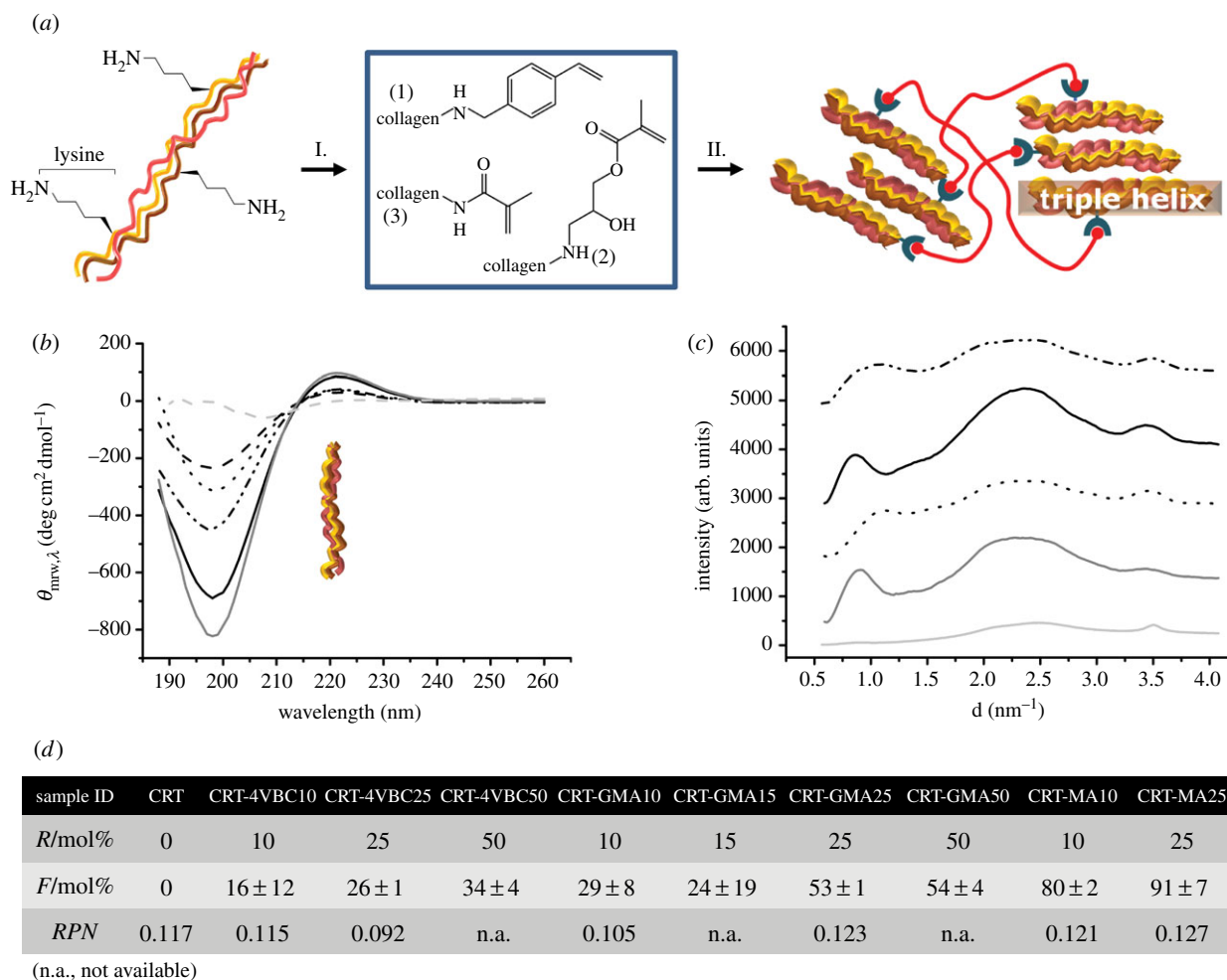
Figure 1. (a) Collagen lysines are covalently functionalized with vinyl moieties, i.e. 4VBC (1), GMA (2) and MA (3), respectively (I); UV irradiation leads to the formation of a covalent hydrogel network (II). (b) CD spectra of samples: gelatin (light grey dashed line), CRT (grey solid line), CRT-MA10 (black dotted line), CRT-MA25 (black dashed line), CRTGMA25 (black solid line), CRT-4VBC25 (black double dot-dashed line). The 221 nm peak is clearly detected in all collagen spectra, revealing the presence of triple helices in functionalized precursors. (c) WAXS spectra of samples: gelatin (light grey dashed line), CRT (grey solid line), CRT-MA10* (black dotted line), CRT-GMA50* (black solid line) and CRT-4VBC25* (black double dotted-dashed line). The WAXS peak ($d \sim 1.1$ nm; $2\Theta \sim 8°$) related to molecular packing of collagen can still be observed in photo-activated systems, resulting in at least 70% retention of native collagen triple helices. (d) Molar excess of monomer with respect to collagen lysines (R), degree of collagen functionalization (F) and CD ratio (RPN) between positive and negative magnitudes are provided for each functionalized collagen formulation. (Online version in colour.)

with previous WAXS quantifications in gelatin samples [58]. These CD and WAXS results therefore provided supporting evidence that obtained functionalized and photo-activated collagen systems displayed only slightly altered triple helical organization with respect to the case of native rat tail type I collagen, despite the fact that covalent functionalization of lysine could be accomplished with varied monomers and tunable degrees of functionalization.

3.2. Morphology, swelling and compression properties

Following investigation of the molecular architecture in functionalized precursors and networks, attention moved to the characterization of photo-activated collagen hydrogels. Functionalized collagen solutions proved to promptly result in a gel following UV irradiation. Formed hydrogels displayed a micro-porous architecture as revealed by SEM (figure 2a,b), whereby reconstituted collagen-like fibrils were expected to form the scaffold struts [22]. The presence of micro-pores (P: 35 ± 7 µm) is appealing for wound dressing applications, since the wound exudate is expected to diffuse within the pores, resulting in increased permeation and exudate

absorbency [59]. Likewise, the presence of micro-pores would also be advantageous for cell culture applications, since pores are expected to facilitate proliferation of cells and diffusion of nutrients within the materials [21].

Besides optical and SEM observations, the macroscopic mechanical properties of formed hydrogels were also addressed. As observed in figure 2c, the SR was determined; all hydrogel systems displayed very high SR values ($SR >$ 700 wt%), with 4VBC-based hydrogels swelling more ($1600 \pm 224 - 1996 \pm 182$ wt%) than GMA- ($851 \pm 52 - 1363 \pm 70$ wt%) and MA-based ($707 \pm 51 - 1087 \pm 96$ wt%) hydrogels. Exemplarily, SR was not found to change significantly when collagen networks CRT-MA10* were equilibrated in PBS instead of water (SR: 1190 ± 34 wt%; figure 2c); this suggests that the presence of a covalent network makes the collagen hydrogel insensitive to changes in solution pH and ionic strength, in agreement with previous results on reconstituted collagen fibrils [37,41]. The molar excess of monomer/Lys employed to accomplish functionalized collagen precursors was found to rule the swelling behaviour of hydrogels CRT-(G)MA*, while the SR of samples CRT-4VBC* did not show significant variations. Figure 1d previously proved that variations in monomer/Lys
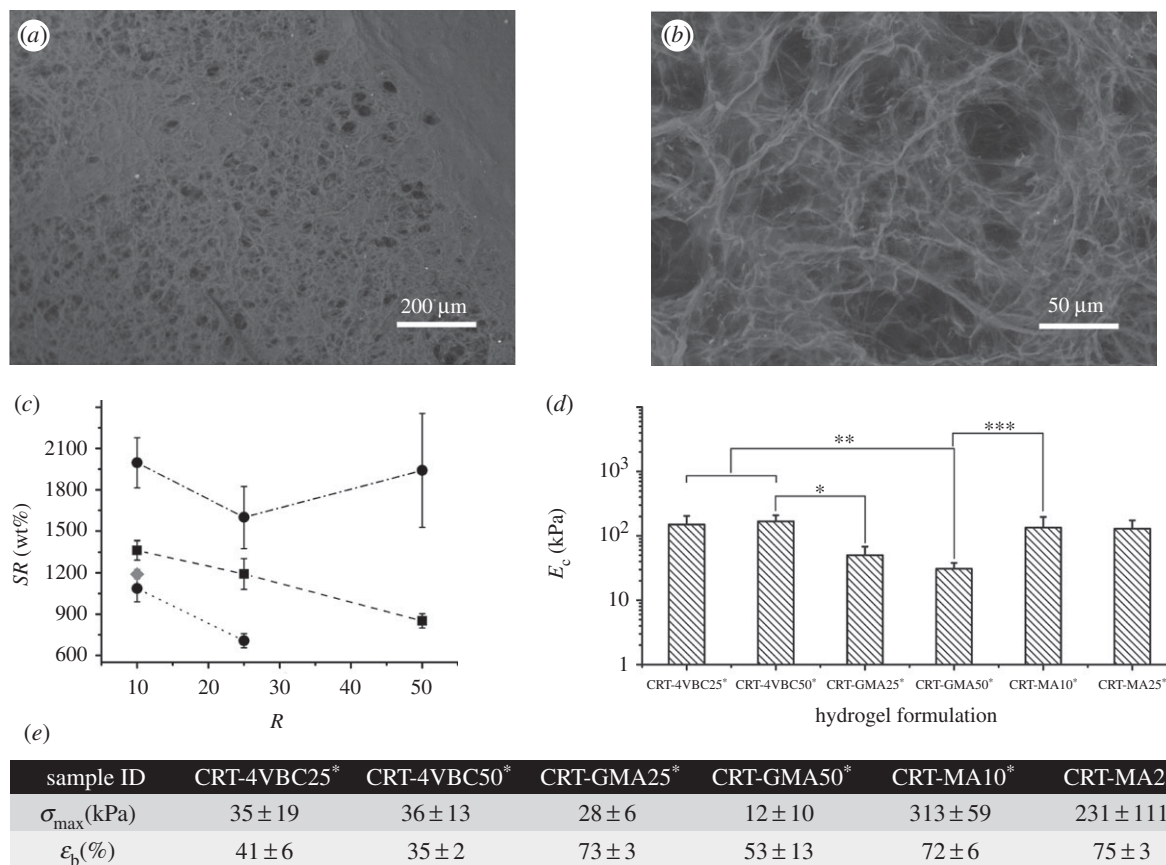
Figure 2. Exemplary SEM images of collagen hydrogel (CRT-GMA50[*]) following network equilibration in 25°C distilled water (a: ×100, b: ×1000). (c) SR of collagen hydrogels synthesized with varied molar excess of monomer with respect to lysine content (R) and incubated in distilled water. Dashed-dotted line, CRT-4VBC[*]; dashed line with squares, CRT-GMA[*]; dotted lines with circles, CRT-MA[*]. Swelling of hydrogel CRT-MA10[*] (grey diamond) was exemplarily measured in PBS instead of distilled water. (d) Compressive moduli (E_c) of collagen hydrogels; '*', '**' and '***' indicate that E_c means of corresponding samples are significantly different (at the 0.05 level, Bonferroni test). (e) Maximal stress (σ_{max}) and compression at break (ϵ_b) measured during hydrogel compression.

sample ID	CRT-4VBC25[*]	CRT-4VBC50[*]	CRT-GMA25[*]	CRT-GMA50[*]	CRT-MA10[*]	CRT-MA25[*]
σ_{max} (kPa)	35 ± 19	36 ± 13	28 ± 6	12 ± 10	313 ± 59	231 ± 111
ϵ_b (%)	41 ± 6	35 ± 2	73 ± 3	53 ± 13	72 ± 6	75 ± 3

molar excess during the functionalization reaction resulted in adjusted degrees of functionalization in precursors CRT-(G)MA, while a nearly constant F was determined in 4VBC-based products, regardless of the reaction conditions. Observed trends in swelling behaviour therefore reflected the extent of lysine derivatization imparted with collagen functionalization, so that an inverse relationship between F (in the collagen precursors) and SR (in the resulting hydrogels) was found. Such inverse F–SR relationships demonstrated that the functionalization step was key to the formation of collagen networks, whereby an increased content of attached vinyl moieties in collagen precursors effectively led to the formation of hydrogels with an increased degree of cross-linking and decreased SR.

Despite the high SR values observed, resulting materials were still highly stable in an aqueous environment, with significantly higher compression modulus (E_c: 150 ± 54–168 ± 40 kPa) and smaller compression at break (ϵ_b: 35 ± 2–41 ± 6%) observed in 4VBC-based, with respect to GMA-based, systems (E_c: 30 ± 7–50 ± 18 kPa; ϵ_b: 53 ± 13–73 ± 3%), while hydrogels CRT-MA[*] displayed intermediate compressive moduli (E_c: 129 ± 45–134 ± 62 kPa) (figure 2d,e). Remarkably, the results showed a direct SR–E_c relationship in hydrogels CRT-4VBC[*], which is rather unexpected given that mechanical properties are supposed to decrease in hydrogels with increased SR and decreased degree of functionalization/cross-linking [39], as found in hydrogels CRT-(G)MA[*]. While the higher SR values could be explained in samples CRT-4VBC[*] in light of their lower degree of functionalization in comparison with methacrylated hydrogel

networks, the compression properties were also increased in aromatic collagen systems. These observations speak against classical rubbery elasticity theories describing synthetic polymer networks [1–5]; we hypothesized that the molecular organization and secondary interactions make additional contributions to the mechanical properties of aromatic collagen systems. We have previously demonstrated that the triple helix conformation can be preserved in functionalized collagen depending on the type and extent of functionalization (figure 1c) [44]. In the case of networks CRT-4VBC[*], the inter-strand physical cross-links between the C=O and N–H groups in the triple helical structure could no longer be mediated following incorporation of the aromatic backbone [20,44,57], as suggested by RPN values deriving from corresponding CD spectra (figure 1b,d). Consequently, the resulting free-standing collagen chains were likely to form new hydrogen bonds with water, thereby explaining the increased SR measured in samples CRT-4VBC[*] (figure 1d). At the same time, the incorporation of the stiff, aromatic 4VBC segment was supposed to play a major role in the compression behaviour of corresponding hydrogels. Aromatic moieties can mediate additional π–π stacking interactions [60,61], so that additional and reversible junction knots could be established during material compression, owing to the vicinity of network chains. The presence of these additional junction knots together with considerations on the molecular stiffness of the introduced aromatic backbone was likely to count for the significant increase in compressive modulus and decrease in strain at break in comparison with hydrogels

based on non-aromatic cross-linking segments. Consequently, the molecular architecture of the collagen networks was found to significantly affect both compression and swelling properties, suggesting that material properties could be adjusted in order to meet specific clinical requirements.

The exceptionally high SR values and compressive moduli of the presented collagen hydrogels make these systems particularly attractive for wound dressing applications, since both properties are crucial but challenging material requirements for successful moist wound healing [40]. An ideal wound dressing should display swelling and mechanical properties adjusted for each type of wound [17,62]. Alginate non-woven fabrics have been proposed as wound or burn dressings, whereby a water absorbency (related to contributions of both bound and unbound water) greater than 25 g of deionized water per gram of fabric was observed [63].

In order to further investigate the relevance of the presented collagen hydrogels in wound care, benchmarking experiments were carried out against a carboxymethylated cellulose-based non-woven dressing (Aquacel), as optimal fibrous material for the management of exudative wounds [62,64]; remarkably, higher values of SR and E_c were observed in collagen hydrogels CRT-4VBC* with respect to the non-woven material (SR: 1759 ± 107; E_c: 34 ± 18 kPa). Together with the observed viability of 5-chloromethylfluorescein-stained L929 fibroblasts following cell culture on collagen hydrogels (electronic supplementary material, figure S3 (left)) as well as the spread-like cell morphology of L929 cells following cell culture with material extract (electronic supplementary material, figure S3 (right)), the above-mentioned observations provide supporting evidence of the potential applicability of these hydrogels as a material building block for the design of advanced wound dressings. In light of these results, current investigations are focusing on the design of collagen non-wovens based on functionalized collagen precursors.

3.3. Atomic force microscopy study

When designing biomaterials, such as wound dressings or tissue scaffolds, it is important that the mechanical properties match the requirements of the intended application. Four distinct contributions were expected to rule the overall mechanical properties in collagen hydrogels: (i) internal microstructure, (ii) molecular architecture of the covalent network, (iii) molecular organization of the protein building block, and (iv) inherent mechanical properties of the hydrogel phase. In this study, we have so far investigated points (i) (figure 2a,b) and (ii) (figure 1b,d), while point (iii) was partially addressed for the triple helical structural ordering at short length scales using CD and WAXS on collagen precursors and networks following functionalization with MA (figure 1c) as well as GMA and 4VBC [44]. In order to fully address points (iii) and (iv) and gain an overall understanding of the governing structure–property relationships, we envisioned a sample preparation method to probe hydrogel micro-mechanical properties via AFM, whereby the presence of any long-range fibrillar structural ordering was also elucidated. AFM on such highly swollen materials is very challenging, considering (i) the material softness, imposing the demand for relatively low load resolution testing; (ii) the large amount of water bound to the material, limiting reliable material fixation on a substrate; and (iii) the material heterogeneity resulting from the inner micro-pores and large surface roughness, potentially leading to resolution

artefacts. In order to address these challenges, water-equilibrated networks were fixed on microscope glass slides via application of a photo-curable adhesive, so that AFM mechanical and structural analyses could be performed (figure 3a–c). Distinct force-indentation plots on hydrogel CRT-MA10* were successfully acquired using a conical indenter with force volume mode, describing a local elastic response with no detectable permanent plastic deformation (figure 3, bottom left) similar to the behaviour observed in hydrated collagen fibrils [36,37]. Here, the presence of the covalent network at the molecular level was mostly responsible for the elastic recovery from the nano- to the macro-scale [24], as also supported by the minimal adhesion and small amount of hysteresis (approx. attojoule; electronic supplementary material, figure S4) between the approach and retraction indentation curves.

The elastic modulus was extracted from the force-indentation curves using the Hertzian model, giving confirmation that the ranges of compression properties observed at the macroscopic scale were correlated to those at smaller length scales. Furthermore, AFM indentation carried out in two separate regions resulted in similar distributions of elastic modulus (figure 3, bottom centre). Both results provided evidence that the sample preparation method ensured complete fixation of the hydrogel to the supporting glass substrate, so that meaningful information on the mechanical and surface properties could be obtained.

Following validation of the AFM experimental set-up, each hydrogel system was analysed. Figure 4a displays the results of E_{AFM} in samples CRT-4VBC*. Obtained E_{AFM} values were comparable to the elastic moduli determined via bulk compression tests. Additionally, no significant variation of nano- to micromechanical properties was measured between samples CRT-4VBC10* and CRT-4VBC25* (E_{AFM}: $237 \pm 77 \rightarrow 374 \pm 36$ kPa), which was expected because of the comparable bulk compressive modulus (macro-scale), on the one hand, and the nearly constant degree of functionalization in respective collagen precursors (figure 1e), on the other hand. While similar mechanical properties were also found in samples CRT-4VBC50* (figure 4b), a large regional variation of E_{AFM} was observed (E_{AFM}: $100 \pm 48 \rightarrow 387 \pm 66$ kPa). In principle, these results may derive from the non-homogeneous material surface, i.e. surface roughness, as revealed by the corresponding height and phase images taken in tapping mode under water (figure 4c,d) and respective height profile (figure 4e). The AFM elastic modulus is generally affected by the surface roughness, given that the interaction volume between the tip and the sample changes depending on how many surface protrusions are in contact with the tip [65]. By comparing surface heterogeneities among hydrogels, however, larger roughness values (R_a: 31 nm; R_q: 20 nm; table 1) were determined on hydrogel CRT-4VBC25* with respect to hydrogel CRT-4VBC50* (R_a: 13 nm; R_q: 16 nm; table 1), despite larger E_{AFM} regional variations being observed in the latter compared with the former sample. Furthermore, force mapping indentation depths ($h > 100$ nm) proved to be much higher than the surface roughness of corresponding hydrogels, suggesting that surface effects played only a minimal role [65].

It was therefore unlikely that roughness effects could account for the observed variations in mechanical properties. Given that these hydrogels resulted from the formation of a molecular covalent network, small localized variations in the cross-linking density were therefore expected to be mostly responsible for the above observation. Collagen hydrogel
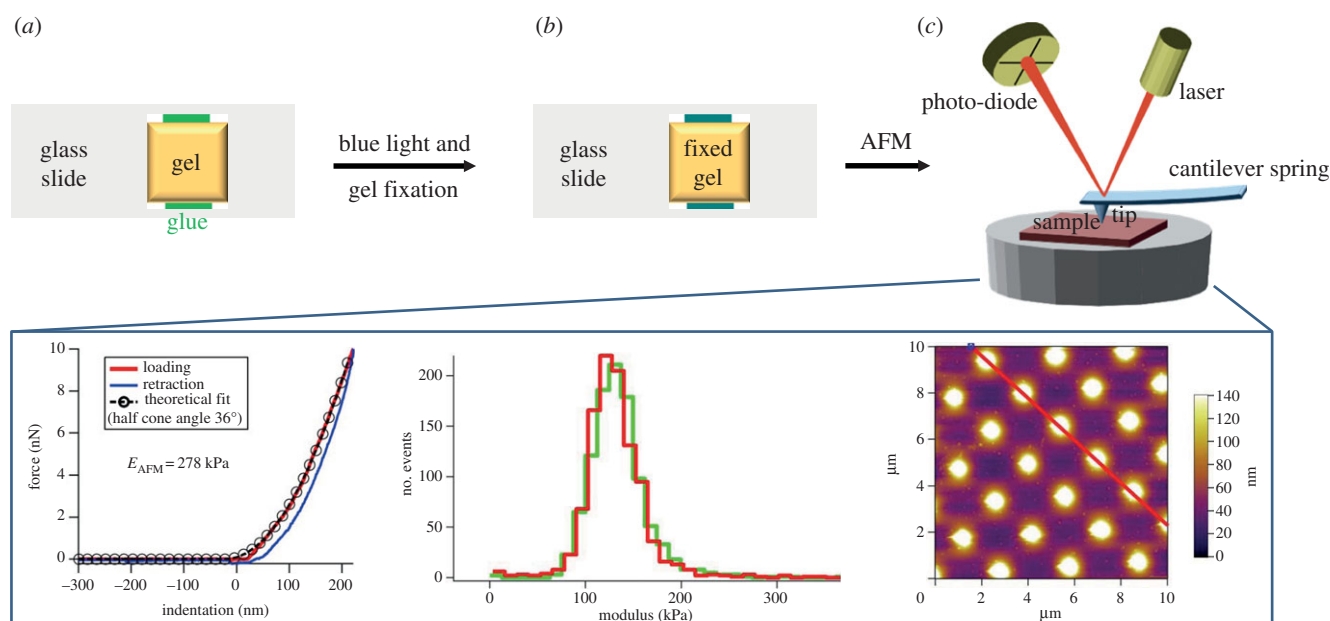
Figure 3. Sample preparation for AFM. (*a*) A microscope glass slide is coated with a photo-curable adhesive above which the collagen hydrogel is laid. (*b*) Blue light is applied to the slide so that the hydrogel is fixed. (*c*) The hydrogel-bearing slide is analysed via AFM. Bottom (from left to right): exemplary AFM force-indentation curve deriving from conical indentation on hydrogel CRT-MA10*; elastic modulus distributions obtained with 3 nN indentation force in two different regions of hydrogel CRT-MA10*; AFM image of a standard tip calibration grid with an array of sharp conical spikes. (Online version in colour.)

networks were indeed obtained via the photo-activation of functionalized collagen molecules, whereby network molecular defects can occur during the photo-cross-linking reaction. The localized variations in cross-linking density are also in agreement with the fact that such variability in elastic modulus was mainly detected at the nano- to micro-scale rather than at the macro-scale (figure 2*d*). Overall, these nano-mechanical investigations suggested that changes in the molecular architecture of the collagen networks dictated the overall mechanical behaviour of resulting hydrogels, while surface topography mainly played a contribution at smaller length scales.

Together with force mapping, AFM imaging was carried out in order to explore the protein organization of functionalized triple helical collagen molecules at the hydrogel surface. As depicted in figure 4*c,d*, no detectable presence of renatured collagen-like fibrils was displayed in samples CRT-4VBC50*. This observation was also supported by obtained roughness values, which were much lower than those of fibrillar surfaces in the sclera (R_q: 60–200 nm) [65]. The fact that no fibril could be revealed by the obtained AFM images could be mostly explained by the specific solvent applied for hydrogel preparation; 4VBC-functionalized collagen precursors were dissolved in diluted acidic conditions (10 mM HCl), whereby no fibrillogenesis could occur and only collagen triple helices were expected to be present in the solution [66]. Following hydrogel formation, the resulting triple helices were therefore frozen in a cross-linked state, so that minimal fibrillar renaturation could be induced even at neutral or basic pH, as confirmed via AFM imaging (figure 4*c,d*).

Further to the investigation on samples CRT-4VBC*, hydrogels CRT-GMA* were addressed. Good agreement between E_{AFM} and E_c values was still observed (figure 5*a,c,e*), whereby hydrogel formulation seemed to affect the mechanical properties of corresponding hydrogels, in contrast to the case of hydrogels CRT-4VBC*. This latter point could result from the fact that GMA-functionalized collagen precursors displayed

a wider variation in the degree of collagen functionalization (F_{GMA}: $29 \pm 8 \rightarrow 54 \pm 4$ mol%; figure 1*d*), unlike the case of hydrogels CRT-4VBC* (F_{4VBC}: $16 \pm 12 \rightarrow 34 \pm 4$ mol%; figure 1*d*). Other than that, a significant regional variation of E_{AFM} was measured in hydrogel CRT-GMA50* (figure 5*e*), as already observed in hydrogel CRT-4VBC50*. In order to explain these results, surface roughness values (table 1), AFM maps (figure 5*e,f*) and SEM images (figure 2*a,b*) were considered. The corresponding surface roughness (R_a: 113 ± 24 nm; R_q: 141 ± 27 nm) was about one order of magnitude higher than that of samples CRT-4VBC50*, suggesting that surface effects may be responsible for E_{AFM} variation. As observed previously, the surface roughness gives an indication of the degree of fibrillogenesis in collagen materials [65]. Evidence of fibrillar organization was observed in AFM height maps of these highly hydrated collagen hydrogels (figure 5*d,f*), in line with the hypothesis that renatured fibrils formed the solid phase of the scaffold (figure 2*a,b*). These considerations were also supported by the fact that these hydrogels were prepared in PBS (unlike the case of hydrogels CRT-4VBC*), which is a common medium applied to induce fibrillogenesis of collagen triple helices [66]. From these considerations, it was therefore likely that surface roughness effects together with the presence of a heterogeneous microstructure consisting of pores and regenerated collagen fibrils could count for the significant variation in AFM-probed mechanical properties.

Comparing hydrogels CRT-GMA15* and CRT-4VBC25*, as based on collagen precursors showing a comparable degree (i.e. F_{GMA}: 24 ± 19 mol%, F_{4VBC}: 26 ± 1 mol%; figure 1*d*), but different type, of functionalization (i.e. GMA- versus 4VBC-based), a decreased elastic modulus was observed in the former system throughout the sample (figure 5*b,c,g*). Given that the two hydrogels were obtained from precursors with a comparable degree of functionalization ($F_{GMA} = 24 \pm 19$ mol%; $F_{4VBC} = 26 \pm 1$ mol%; figure 1*d*), the most probable explanation for this observation was that the backbone stiffness of cross-linking segments directly affected the mechanical
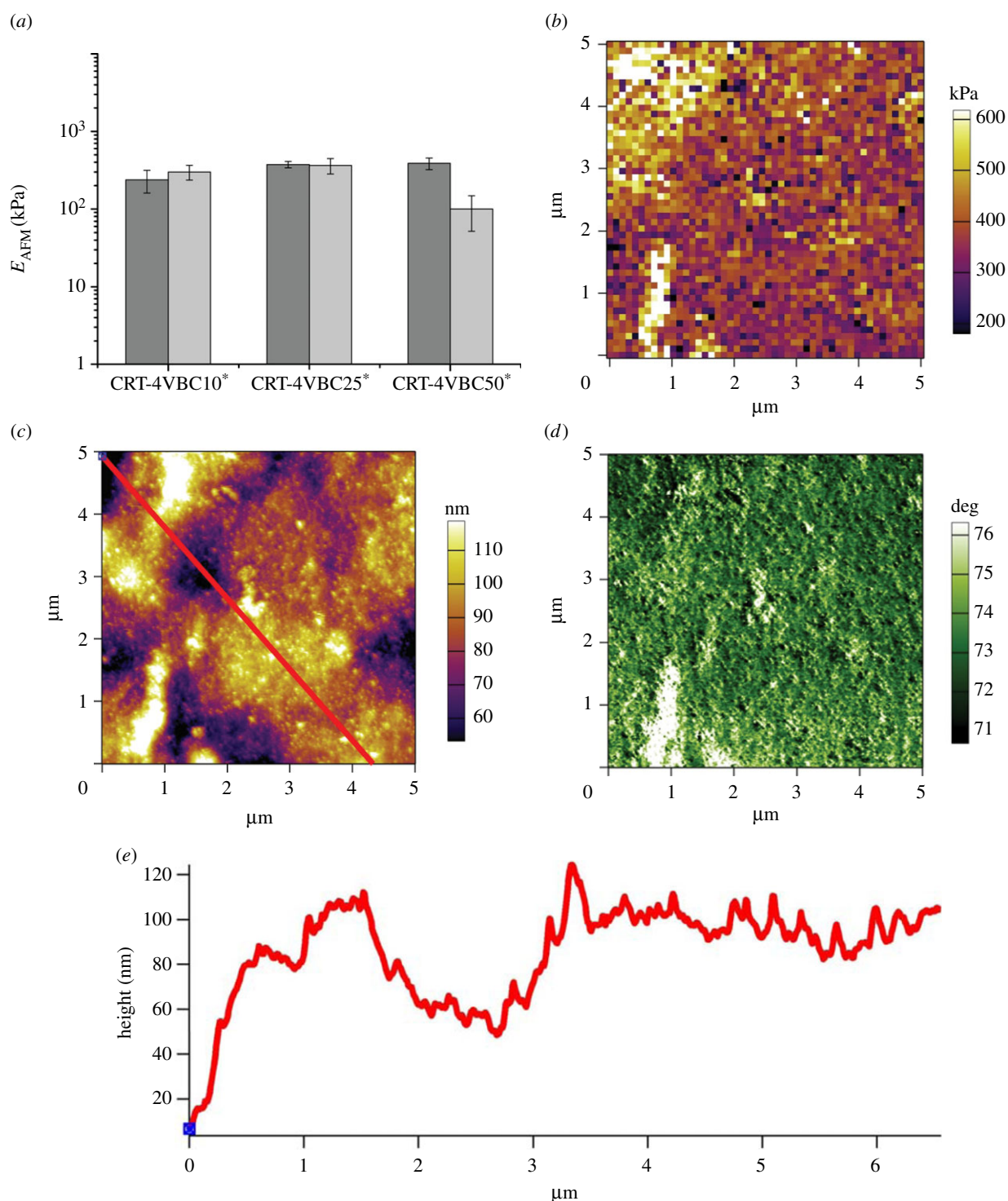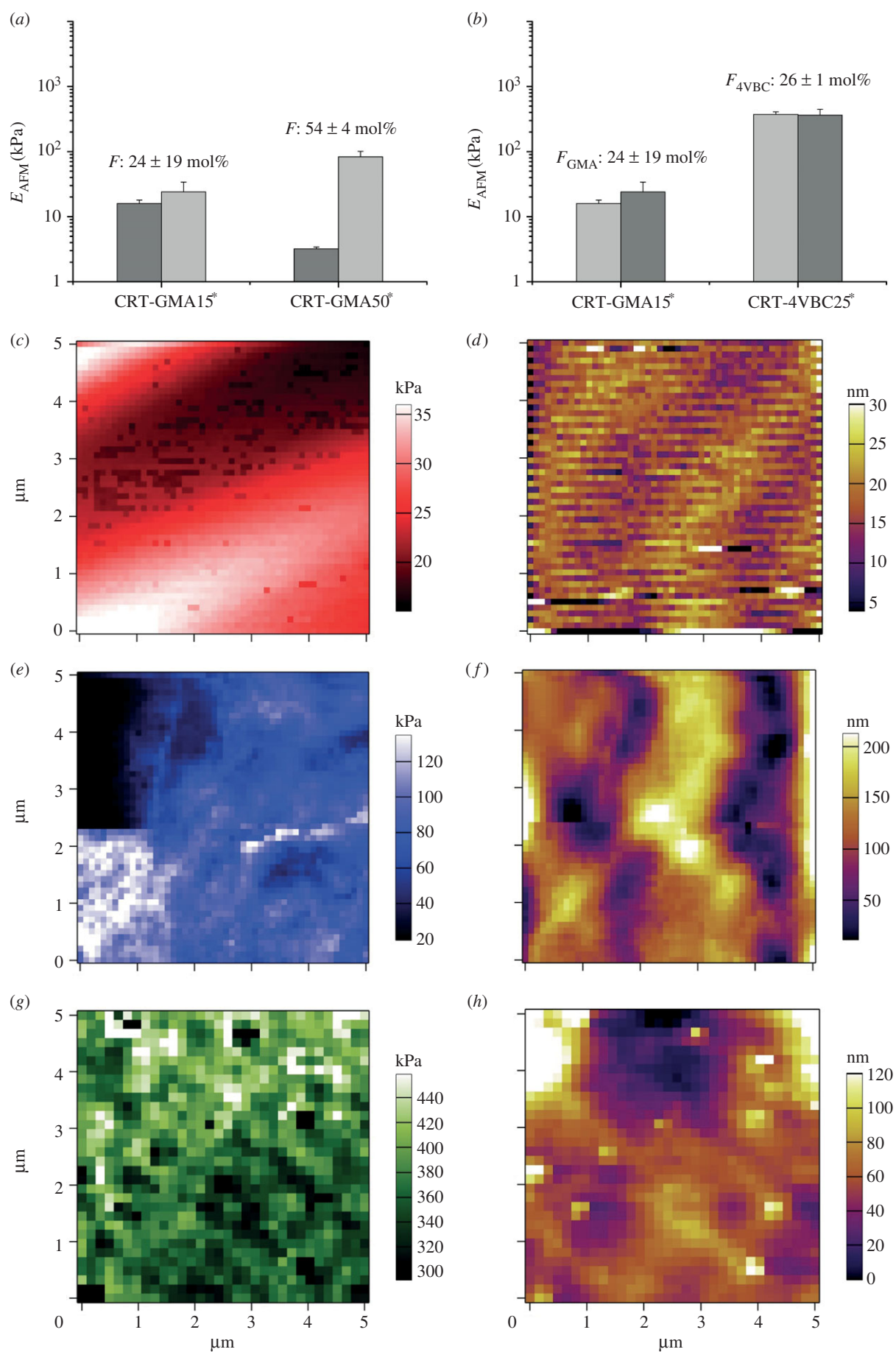
Figure 4. (*a*) Variation of E_{AFM} in hydrogels CRT-4VBC[*] determined via AFM indentation. Two replicates were used for sample CRT-4VBC10[*], while two different regions in the same replica were investigated for the other two sample formulations. (*b–d*) Exemplary E_{AFM} map (*b*, 5 nN indentation force), surface image (*c*) and phase tapping mode image (*d*) obtained in hydrogel CRT-4VBC50[*]. As expected, no collagen fibrils could be observed on the material surface, since these hydrogels were prepared in 10 mM HCl solution, with which no fibrillogenesis can occur. (*e*) Height profile determined along the cross line section of figure 2*c*. (Online version in colour.)

Table 1. Mean (R_a) and root mean square (R_q) roughness values obtained in collagen hydrogels via AFM. R_a and R_q were computationally calculated from AFM height data on a 5×5 μm scan size.

| sample ID	CRT-4VBC25[*]	CRT-4VBC-50[*]	CRT-GMA15[*b]	CRT-GMA50[*a]	CRT-MA10[*]
R_a (nm)	31	13	3 ± 1	113 ± 24	36
R_q (nm)	20	16	4 ± 1	141 ± 27	46

[a]Height maps ($n = 4$) were generated from E_{AFM} maps using the indentation contact point.
[b]Two height maps were obtained for this sample.

Figure 5. (*a*) Variation of E_{AFM} in hydrogels CRT-GMA* with varied degrees of functionalization; (*b*) comparison of E_{AFM} in hydrogels CRT-GMA15* and CRT-4VBC25* displaying comparable degrees of functionalization. Grey and light grey columns are related to different regions of the same sample. (*c,d*) Exemplary E_{AFM} map (*c*) and height map (*d*) of hydrogel CRT-GMA15*. (*e,f*) Exemplary E_{AFM} map (*e*) and height map (*f*) of hydrogel CRT-GMA50*. (*g,h*) Exemplary E_{AFM} map (*g*) and height map (*h*) of hydrogel CRT-4VBC25*. All AFM measurements were carried out with 5 nN indentation force. (Online version in colour.)
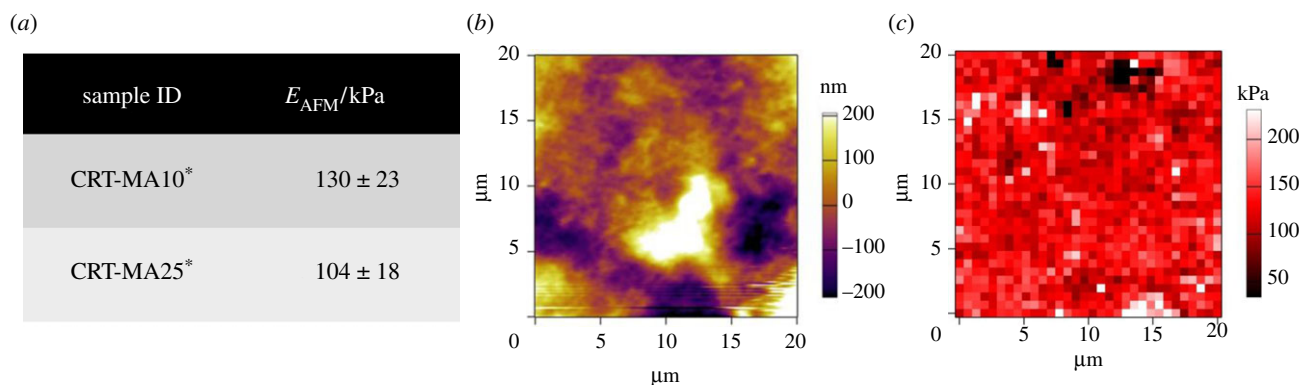
Figure 6. (a) Variation in E_{AFM} in CRT-MA* hydrogels (5×5 μm scan size) with varied degrees of functionalization. (b,c) AFM surface image and E_{AFM} map on hydrogel CRT-MA10*. (Online version in colour.)

properties of the resulting hydrogels, e.g. the incorporation of 4VBC aromatic moieties imparted superior mechanical properties in corresponding networks with respect to GMA-based systems (as observed via the bulk compression measurements). Other than E_{AFM}, the fibril-forming properties of functionalized collagen molecules in hydrogels CRT-GMA15* (figure 5d) and CRT-4VBC25* (figure 5h) appeared to be different. Evidence of long-range structural assemblies was found in the former system similarly to the case of CRT-GMA50*, although this was not supported via the roughness data (table 1); other than that, a random organization was apparent in the case of hydrogel CRT-4VBC25* (as already shown in hydrogel CRT-4VBC50*). Given that these hydrogels were prepared in different solutions, these observations provided supporting evidence of the effect the solvent, e.g. with respect to the solution pH, employed during hydrogel preparation can have on the fibrillar renaturation of functionalized collagen precursors.

Following AFM investigation on samples CRT-4VBC* and CRT-GMA*, attention moved to the characterization of hydrogels CRT-MA*, whereby mechanical properties, surface images and E_{AFM} maps were measured. The resulting hydrogels displayed an averaged E_{AFM} of around 104–130 kPa (figure 6a), which was comparable to the value observed via compression (E_c: 129–134 kPa) and between E_{AFM} values of hydrogels CRT-GMA* (figure 5a) and CRT-4VBC* (figure 4a). At the same time, E_{AFM} was nearly constant among samples regardless of the hydrogel formulations, which was expected because of the slight variation in the degree of functionalization in corresponding collagen precursors. Comparing the three sets of hydrogel systems, hydrogels CRT-MA* displayed a much higher degree of functionalization than hydrogels CRT-GMA* (figure 1d), which was likely to explain why the elastic modulus in hydrogels CRT-MA* was higher than that in hydrogels CRT-GMA*. Moreover, both GMA and MA are aliphatic molecules, so the backbone rigidity of resulting cross-linking segments was expected to be similar between the two networks.

Following similar reasoning, the molecular stiffness of the introduced cross-linking segments of collagen molecules was likely to explain the lower elastic modulus observed in hydrogels CRT-MA* with respect to hydrogels CRT-4VBC*, given that the 4VBC-based cross-linking segments were previously confirmed to provide a stiffer junction between collagen molecules with respect to the GMA aliphatic segments. Other than the tunability of E_{AFM} among hydrogels, E_{AFM} values showed a nearly homogeneous regional distribution throughout E_{AFM} maps of hydrogels CRT-MA10* (E_{AFM}: $130 \pm 23 \rightarrow 127 \pm 22$ kPa; figure 3, centre bottom), which was in agreement with the surface roughness values (R_a: 36 nm; R_q: 46 nm; table 1) derived from corresponding surface images (figure 6b). The nearly homogeneous regional distribution of mechanical properties could be explained by a uniform cross-linking density in the corresponding collagen network at the molecular level, in light of the almost quantitative functionalization of collagen lysines ($F_{MA} > 80$ mol%) in respective collagen precursors. In addition, the relatively low values of surface roughness also suggested a low degree of fibrillogenesis in hydrogel CRT-MA10*, as revealed by the AFM surface image (figure 6b). Fibrillogenesis should be expected in this case, since a 73% triple helix content (with respect to native collagen) was determined in this sample via WAXS (figure 1c). Furthermore, hydrogels CRT-MA* were prepared in PBS, which is a solvent promoting renaturation of collagen triple helices into fibrils. The most probable explanation for the absence of collagen fibrils in AFM images was that the higher functionalization degree of MA-functionalized collagen precursors (compared with, for example, the case of GMA-functionalized ones) was likely to strongly affect the kinetics of native collagen fibrillogenesis. Consequently, a longer incubation time under physiological conditions was likely to be required in order to enable MA-functionalized collagen to reconstitute into fibrils. The influence of the degree of collagen functionalization on the fibril-forming capability of the corresponding collagen precursors will be systematically addressed in a different study.

4. Conclusion

Mechanically competent collagen hydrogels were successfully developed from varied photo-active precursors, i.e. CRT-4VBC, CRT-GMA and CRT-MA, and investigated from the molecular up to the macroscopic scale. Photo-active precursors exhibited systematically adjusted degrees of functionalization (F: 16 ± 12–91 ± 7 mol%) depending on the type and feed ratio of the monomer. Because of the changes at the molecular level, the resulting collagen hydrogels displayed wide tunability in bulk compressive modulus (E_c: 30 ± 7–168 ± 40 kPa), which was confirmed by the AFM elastic modulus (E_{AFM}: 16 ± 2–387 ± 66 kPa) measured at the nanoscale. The backbone stiffness of vinyl moieties incorporated in the collagen network was the key factor affecting hydrogel mechanical

and swelling properties. The fibril-forming capability of functionalized collagen molecules was in addition affected by the degree of functionalization. Remarkably, collagen aromatic systems displayed a higher compressive modulus than aliphatic systems of a comparable degree of functionalization, suggesting the establishment of reversible $\pi-\pi$ stacking interactions between the introduced 4VBC aromatic rings. In light of their remarkable *SR* (SR: $707 \pm 51-1996 \pm 182$ wt%) and mechanical properties as well as the observed cyto-compatibility with mouse fibroblasts, these collagen hydrogels have widespread potential for clinical applications in chronic wound care and regenerative medicine and are also highly suitable as biomimetic niches for stem cell differentiation.

References

1. Slaughter BV, Khurshid SS, Fisher OZ, Khademhosseini A, Peppas N. 2009 Hydrogels in regenerative medicine. *Adv. Mater.* **21**, 3307–3329. (doi:10.1002/adma.200802106)

2. Kirschner CM, Anseth KS. 2013 Hydrogels in healthcare: from static to dynamic material microenvironments. *Acta Mater.* **61**, 931–944. (doi:10.1016/j.actamat.2012.10.037)

3. Wichterle O, Lim D. 1960 Hydrophilic gels for biological use. *Nature* **185**, 117–118. (doi:10.1038/185117a0)

4. Koehler KC, Anseth KS, Bowman CN. 2013 Diels-Alder mediated controlled release from a poly[ethylene glycol] based hydrogel. *Biomacromolecules* **14**, 538–547. (doi:10.1021/bm301789d)

5. Chong SF, Smith AAA, Zelikin AN. 2013 Microstructured, functional PVA hydrogels through bioconjugation with oligopeptides under physiological conditions. *Small* **9**, 942–950. (doi:10.1002/smll.201201774)

6. Jeon O, Powell C, Solorio LD, Krebs MD, Alsberg E. 2011 Affinity-based growth factor delivery from biodegradable, photocrosslinked heparin-alginate hydrogels. *J. Control. Rel.* **154**, 258–266. (doi:10.1016/j.jconrel.2011.06.027)

7. Shingel KI, Di Stabile L, Marty JP, Faure MP. 2006 Inflammatory inert poly[ethylene glycol]–protein wound dressing improves healing responses in partial- and full-thickness wounds. *Int. Wound J.* **3**, 332–342. (doi:10.1111/j.1742-481X.2006.00262.x)

8. Phelps EA, Headen DM, Taylor WR, Thulé PM, García AJ. 2013 Vasculogenic bio-synthetic hydrogel for enhancement of pancreatic islet engraftment and function in type 1 diabetes. *Biomaterials* **34**, 4602–4611. (doi:10.1016/j.biomaterials.2013.03.012)

9. Cha C, Shin SR, Gao X, Annabi N, Dokmeci MR, Tang X, Khademhosseini A. 2014 Controlling mechanical properties of cell-laden hydrogels by covalent incorporation of graphene oxide. *Small* **10**, 514–523. (doi:10.1002/smll.201302182)

10. Mano JF *et al.* 2007 Natural origin biodegradable systems in tissue engineering and regenerative medicine: present status and some moving trends. *J. R. Soc. Interface* **4**, 999–1030. (doi:10.1098/rsif.2007.0220)

11. Tronci G, Ajiro H, Russell SJ, Wood DJ, Akashi M. 2014 Tunable drug-loading capability of chitosan hydrogels with varied network architectures. *Acta Biomater.* **10**, 821–830. (doi:10.1016/j.actbio.2013.10.014)

12. Bencherif SA, Sands RW, Bhatta D, Arany P, Verbeke CS, Edwards DA, Mooney DJ. 2012 Injectable preformed scaffolds with shape-memory properties. *Proc. Natl Acad. Sci. USA* **109**, 19 590–19 595. (doi:10.1073/pnas.1211516109)

13. Huynh T, Abraham G, Murray J, Brockbank K, Hagen P-O, Sullivan S. 1999 Remodeling of an acellular collagen graft into a physiologically responsive neovessel. *Nat. Biotechnol.* **17**, 1083–1086. (doi:10.1038/15062)

14. Davidenko N, Gibb T, Schuster C, Best SM, Campbell JJ, Watson CJ, Cameron RE. 2012 Biomimetic collagen scaffolds with anisotropic pore architecture. *Acta Biomater.* **8**, 667–676. (doi:10.1016/j.actbio.2011.09.033)

15. Lin J, Li C, Zhao Y, Hu J, Zhang L-M. 2012 Co-electrospun nanofibrous membranes of collagen and zein for wound healing. *ACS Appl. Mater. Interfaces* **4**, 1050–1057. (doi:10.1021/am201669z)

16. Jones V, Grey JE, Harding KG. 2006 Wound dressings. *Br. Med. J.* **332**, 777–780. (doi:10.1136/bmj.332.7544.777)

17. Boateng JS, Matthews KH, Stevens HNE, Eccleston GM. 2007 Wound healing dressings and drug delivery systems: a review. *J. Pharm. Sci.* **97**, 2892–2923. (doi:10.1002/jps.21210)

18. Balakrishnan B, Mohanty M, Umashankar PR, Jayakrishnan A. 2005 Evaluation of an in situ forming hydrogel wound dressing based on oxidized alginate and gelatin. *Biomaterials* **26**, 6335–6342. (doi:10.1016/j.biomaterials.2005.04.012)

19. Adhirajan N, Shanmugasundaram N, Shanmuganathan S, Babu M. 2009 Functionally modified gelatin microspheres impregnated collagen scaffold as novel wound dressing to attenuate the proteases and bacterial growth. *Eur. J. Pharm. Sci.* **36**, 235–245. (doi:10.1016/j.ejps.2008.09.010)

20. Harley BA, Leung JH, Silva ECCM, Gibson LJ. 2007 Mechanical characterization of collagen-glycosaminoglycan scaffolds. *Acta Biomater.* **3** 463–474. (doi:10.1016/j.actbio.2006.12.009)

21. Schmidt JJ, Jeong JH, Chan V, Cha C, Baek K, Lai M-H, Bashir R, Kong H. 2013 Tailoring the dependency between rigidity and water uptake of a microfabricated hydrogel with the conformational rigidity of a polymer cross-linker. *Biomacromolecules* **14**, 1361–1369. (doi:10.1021/bm302004v)

22. Bishop SM, Walker M, Rogers AA, Chen WYJ. 2003 Importance of moisture balance at the wound-dressing interface. *J. Wound Care* **12**, 125–128. (doi:10.12968/jowc.2003.12.4.26484)

23. Lee SM, Pippel E, Moutanabbir O, Gunkel I, Thurn-Albrecht T, Knez M. 2010 Improved mechanical stability of dried collagen membrane after metal infiltration. *ACS Appl. Mater. Interfaces* **2**, 2436–2441. (doi:10.1021/am100438b)

24. Ferreira AM, Gentile P, Chiono V, Ciardelli G. 2012 Collagen for bone tissue regeneration. *Acta Biomater.* **8**, 3191–3200. (doi:10.1016/j.actbio.2012.06.014)

25. Agostini de Moraes M, Paternotte E, Mantovani D, Masumi Beppu M. 2012 Mechanical and biological performances of new scaffolds made of collagen hydrogels and fibroin microfibers for vascular tissue engineering. *Macromol. Biosci.* **12**, 1253–1264. (doi:10.1002/mabi.201200060)

26. Tiller JC, Bonner G, Pan L-C, Klibanov AM. 2001 Improving biomaterial properties of collagen films by chemical modification. *Biotechnol. Bioeng.* **73**, 246–252. (doi:10.1002/bit.1057)

27. Haugh MG, Murphy CM, McKiernan RC, Altenbuchner C, O'Brien F. 2011 Crosslinking and mechanical properties significantly influence cell attachment, proliferation, and migration within collagen glycosaminoglycan scaffolds. *Tissue Eng. Part A* **9–10**, 1202–1208.

28. Fathima NN, Baias M, Blumich B, Ramasami T. 2010 Structure and dynamics of water in native and tanned collagen fibers: effect of crosslinking. *Int. J. Biol. Macromol.* **47**, 590–596. (doi:10.1016/j.ijbiomac.2010.08.003)

29. Hartwell R, Leung V, Chavez-Munoz C, Nabai L, Yang H, Ko F, Ghahary A. 2011 A novel hydrogel-collagen composite improves functionality of an injectable extracellular matrix. *Acta Biomater.* **7**, 3060–3069. (doi:10.1016/j.actbio.2011.04.024)

30. Klumpp D *et al.* 2012 Three-dimensional vascularization of electrospun PCL/collagen-blend

nanofibrous scaffolds *in vivo*. *J. Biomed. Mater. Res. Part A* **100**, 2302–2311.

31. He L, Mu C, Shi J, Zhang Q, Shi B, Lin W. 2011 Modification of collagen with a natural cross-linker, procyanidin. *Int. J. Biol. Macromol.* **48**, 354–359. (doi:10.1016/j.ijbiomac.2010.12.012)

32. Nam K, Sakai Y, Hashimoto Y, Kimura T, Kishida A. 2012 Fabrication of a heterostructural fibrillated collagen matrix for the regeneration of soft tissue function. *Soft Matter* **8**, 472–480. (doi:10.1039/c1sm06543b)

33. Antoine EE, Vlachos PP, Rylander MN. 2014 Review of collagen I hydrogels for bioengineered tissue microenvironments: characterization of mechanics, structure, and transport. *Tissue Eng Part B* **20**, 1–13.

34. Shen ZL, Kahn H, Ballarini R, Eppell SJ. 2011 Viscoelastic properties of isolated collagen fibrils. *Biophys. J.* **100**, 3008–3014. (doi:10.1016/j.bpj.2011.04.052)

35. Stylianou A, Yova D. 2013 Surface nanoscale imaging of collagen thin films by atomic force microscopy. *Mater. Sci. Eng. C* **33**, 2947–2957. (doi:10.1016/j.msec.2013.03.029)

36. Grant CA, Brockwell DJ, Radford SE, Thomson NH. 2008 Effects of hydration on the mechanical response of individual collagen fibrils. *Appl. Phys. Lett.* **92**, 233902. (doi:10.1063/1.2937001)

37. Grant CA, Brockwell DJ, Radford SE, Thomson NH. 2009 Tuning the elastic modulus of hydrated collagen fibrils. *Biophys. J.* **97**, 2985–2992. (doi:10.1016/j.bpj.2009.09.010)

38. Shen ZL, Dodge MR, Kahn H, Ballarini R, Eppell SJ. 2008 Stress–strain experiments on individual collagen fibrils. *Biophys. J.* **95**, 3956–3963. (doi:10.1529/biophysj.107.124602)

39. Carlisle CR, Coulais C, Guthold M. 2010 The mechanical stress–strain properties of single electrospun collagen type I nanofibers. *Acta Biomater.* **6**, 2997–3003. (doi:10.1016/j.actbio.2010.02.050)

40. Svensson RB, Mulder H, Kovanen V, Magnusson SP. 2013 Fracture mechanics of collagen fibrils: influence of natural crosslinks. *Biophys. J.* **104**, 2476–2484. (doi:10.1016/j.bpj.2013.04.033)

41. Svensson RB, Hassenkam T, Grant CA, Magnusson SP. 2010 Tensile properties of human collagen fibrils and fascicles are insensitive to environmental salts. *Biophys. J.* **99**, 4020–4027. (doi:10.1016/j.bpj.2010.11.018)

42. Svensson RB, Hansen P, Hassenkam T, Haraldsson BT, Aagaard P, Kovanen V, Krogsgaard M, Kjaer M, Magnusson SP. 2012 Mechanical properties of human patellar tendon at the hierarchical levels of tendon and fibril. *J. Appl. Physiol.* **112**, 419–426. (doi:10.1152/japplphysiol.01172.2011)

43. Yunoki S, Matsuda T. 2008 Simultaneous processing of fibril formation and cross-linking improves mechanical properties of collagen. *Biomacromolecules* **9**, 879–885. (doi:10.1021/bm7012058)

44. Tronci G, Russell SJ, Wood DJ. 2013 Photo-active collagen systems with controlled triple helix architecture. *J. Mater. Chem. B* **1**, 3705–3715. (doi:10.1039/c3tb20720j)

45. Ouasti S, Donno R, Cellesi F, Sherratt MJ, Terenghi G, Tirelli N. 2011 Network connectivity, mechanical properties and cell adhesion for hyaluronic acid/PEG hydrogels. *Biomaterials* **32**, 6456–6470. (doi:10.1016/j.biomaterials.2011.05.044)

46. Mironi-Harpaz I, Wang DY, Venkatraman S, Seliktar D. 2012 Photopolymerization of cell-encapsulating hydrogels: crosslinking efficiency versus cytotoxicity. *Acta Biomater.* **8**, 1838–1848. (doi:10.1016/j.actbio.2011.12.034)

47. Lapworth JW, Hatton PV, Goodchild RL, Rimmer S. 2012 Thermally reversible colloidal gels for three-dimensional chondrocyte culture. *J. R. Soc. Interface* **9**, 362–375. (doi:10.1098/rsif.2011.0308)

48. Bubnis WA, Ofner CM. 1992 The determination of epsilon-amino groups in soluble and poorly soluble proteinaceous materials by a spectrophotometric method using trinitrobenzenesulfonic acid. *Analyt. Biochem.* **207**, 129–133. (doi:10.1016/0003-2697(92)90513-7)

49. Hutter JL, Bechhoefer J. 1993 Calibration of atomic-force microscope tips. *Rev. Sci. Instrum.* **64**, 1868–1873. (doi:10.1063/1.1143970)

50. Gaudet ID, Shreiber DI. 2012 Characterization of methacrylated type-I collagen as a dynamic, photoactive hydrogel. *Biointerphases* **7**, 25–34. (doi:10.1007/s13758-012-0025-y)

51. Brinkman WT, Nagapudi K, Thomas BS, Chaikof EL. 2003 Photo-cross-linking of type I collagen gels in the presence of smooth muscle cells: mechanical properties, cell viability, and function. *Biomacromolecules* **4**, 890–895. (doi:10.1021/bm0257412)

52. Maxwell CA, Wess TJ, Kennedy CJ. 2006 X-ray diffraction study into the effects of liming on the structure of collagen. *Biomacromolecules* **7**, 2321–2326. (doi:10.1021/bm060250t)

53. Gonzalez LG, Hiller J, Terrill NJ, Parkinson J, Thomas K, Wess TJ. 2012 Effects of isopropanol on collagen fibrils in new parchment. *Chem. Cent. J.* **6**, 24–30. (doi:10.1186/1752-153X-6-24)

54. Sionkowska A, Wisniewski M, Skopinska J, Kennedy CJ, Wess TJ. 2004 Molecular interactions in collagen and chitosan blends. *Biomaterials* **25**, 795–801. (doi:10.1016/S0142-9612(03)00595-7)

55. Madhan B, Subramanian V, Raghava Rao J, Unni Nair B, Ramasami T. 2005 Stabilization of collagen using plant polyphenol: role of catechin. *Int. J. Biol. Macromol.* **37**, 47–53. (doi:10.1016/j.ijbiomac.2005.08.005)

56. Feng Y, Melacini G, Taulane JP, Goodman M. 1996 Acetyl-terminated and template-assembled collagen-based polypeptides composed of Gly-Pro-Hyp sequences. 2. Synthesis and conformational analysis by circular dichroism, ultraviolet absorbance, and optical rotation. *J. Am. Chem. Soc.* **118**, 10 351–10 358. (doi:10.1021/ja961260c)

57. Hodges JA, Raines RT. 2005 Stereoelectronic and steric effects in the collagen triple helix: toward a code for strand association. *J. Am. Chem. Soc.* **127**, 15 923–15 932. (doi:10.1021/ja054674r)

58. Zaupa A, Neffe AT, Pierce BF, Noechel U, Lendlein A. 2011 Influence of tyrosine-derived moieties and drying conditions on the formation of helices in gelatin. *Biomacromolecules* **12**, 75–81. (doi:10.1021/bm101029k)

59. Khil M-S, Cha D-I, Kim H-Y, Kim I-S, Bhattarai N. 2003 Electrospun nanofibrous polyurethane membrane as wound dressing. *J. Biomed. Mater. Res. Part B: Appl. Biomater.* **67B**, 675–679. (doi:10.1002/jbm.b.10058)

60. Fang L, Park JY, Ma H, Jen AK-Y, Salmeron M. 2007 An atomic force microcopy study of the mechanical and electrical properties of monolayer films of molecules with aromatic end groups. *Langmuir* **23**, 11 522–11 525. (doi:10.1021/la701489p)

61. Silioc C, Maleki A, Zhu K, Kjøniksen AL, Nyström B. 2007 Effect of hydrophobic modification on rheological and swelling features during chemical gelation of aqueous polysaccharides. *Biomacromolecules* **8**, 719–728. (doi:10.1021/bm061090o)

62. Waring MJ, Parsons D. 2001 Physico-chemical characterisation of carboxymethylated spun cellulose fibres. *Biomaterials* **22**, 903–912. (doi:10.1016/S0142-9612(00)00254-4)

63. Mahoney MJ. 1993 *Absorbency alginate fabric, use as wound and burn dressings and a method for its preparation.* US Patent no. US5256477 A.

64. Williams C. 1999 An investigation of the benefits of Aquacel hydrofibre wound dressing. *Br. J. Nursing* **8**, 676–680. (doi:10.12968/bjon.1999.8.10.6607)

65. Grant CA, Thomson NH, Savage MD, Woon HW, Greig D. 2011 Surface characterisation and biomechanical analysis of the sclera by atomic force microscopy. *J. Mech. Behav. Biomed. Mater.* **4**, 535–540. (doi:10.1016/j.jmbbm.2010.12.011)

66. Abou Neel EA, Bozec L, Knowles JC, Syed O, Mudera V, Day R, Hyun JK. 2013 Collagen—emerging collagen based therapies hit the patient. *Adv. Drug Deliv. Rev.* **65**, 429–456. (doi:10.1016/j.addr.2012.08.010)